Characteristics of surface wave Green's function for anisotropic ambient seismic noise field — a case study in Limburg, The Netherlands

Soumen Koley[1]*, Henk Jan Bulten[1], Jo van den Brand[1], Maria Bader[1], Frank Linde[1] and Mark Beker[2] discuss the results of the extracted surface wave Green's function when illuminated by an anisotropic distribution of noise sources.

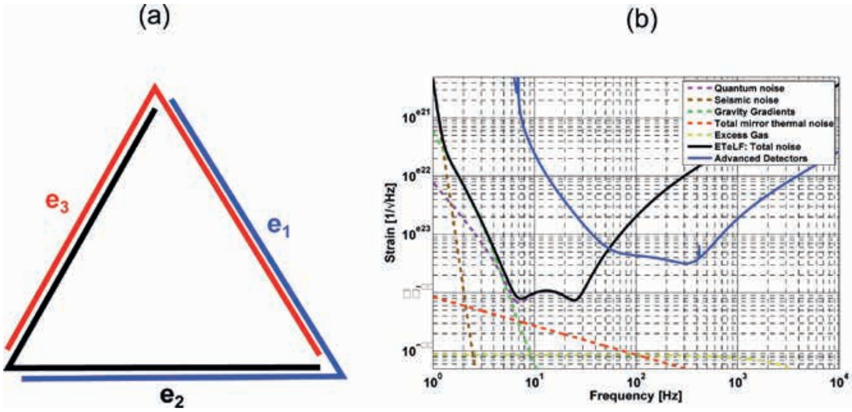

Figure 1 (a) Triangular topology of ET, in which each arm of length L is used twice to form three detectors with a 60° opening angle. (b) Fundamental noise contributions of the xylophone configuration of the ET-LF detector with a circulating power of 18 kW as compared to the sensitivity curve of Advanced Virgo detector shown in blue.

Introduction

The Advanced LIGO and the Advanced Virgo gravitational wave (GW) detectors are built on the surface of the earth. Seismic noise being most dominant on the surface limits the low frequency sensitivity of the detectors below 10 Hz. The Einstein Telescope (ET), a European project for constructing a third generation GW detector aims to improve current detector sensitivity by an order of magnitude at frequencies below 10 Hz. One way of reducing the contribution from seismic noise is by building the detector underground. Currently seismic studies are being conducted in Sardinia, Italy and Limburg, The Netherlands, for selecting an appropriate site for constructing the ET. A dense array of 146 wireless vertical component geophones was deployed at Limburg in The Netherlands with the aim of performing passive seismic tomography using the seismic noise in the frequency band 2.5-8.0 Hz. Theoretically for accurate extraction of surface wave Green's function, an isotropic distribution of noise sources surrounding a station pair is desired. However, in reality the distribution of noise sources manifest azimuthal anisotropy and also vary in source magnitude. In this article, we discuss the results of the accuracy of the extracted surface wave Green's function when illuminated by an anisotropic distribution of noise sources. We make use of the method of cross-correlation beamforming to extract station pairs that yield accurate surface waves Green's function and consequently compute the surface wave group velocities for the region.

Motivation

The current gravitational wave (GW) detector network comprising the two Advanced LIGO detectors and the Advanced Virgo detector have recorded a handful of binary black hole merger events and a binary neutron star merger event (LSC et al., 2018), but they are unlikely to yield a great number of sources, nor sources with very large signal-to-noise ratio (SNR-50) essential requisites for precision astronomy. To do so would necessitate a detector that has improved low frequency sensitivity and greater amplitude sensitivity, a factor 10 in both. Einstein Telescope (ET), a third generation gravitational wave detector was conceived to improve the current sensitivity of detectors by a factor of 10 in the frequency band of 2-10^4 Hz (Puntoro et al., 2010). The ET design study team concluded that a triangular topology is the optimal strategy to achieve the sensitivity goal of a third generation detector (Freise et al., 2009, Freise et al., 2011). The arms of the triangle are each used twice to form three Michelson interferometers as shown in Figure 1a. Each V-shaped detector in the array has L = 10 km arms, with an opening angle of 60° and the detectors are rotated relative to each other by an angle of 120°.

The current second generation ground-based detectors achieved strain sensitivity in the order of $10^{-23} h/\sqrt{Hz}$ in a broad frequency range of 50-1000 Hz. However, significant improvements need to be realized to improve the low frequency sensitivity. As stated earlier, the ET design follows a xylophone

[1] National Institute of Subatomic Physics | [2] Innoseis B.V.
* Corresponding author, E-mail: skoley@nikhef.nl

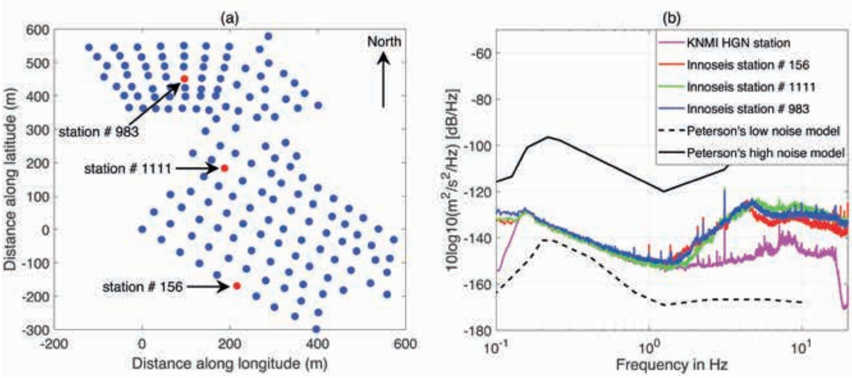

Figure 2 (a) Seismic array layout with three sensors corresponding to the ones for which the PSDs are plotted. (b) Average PSD of vertical ground velocity as measured by the Innoseis stations and that measured at the KNMI HGN station for 20 December, 2017.

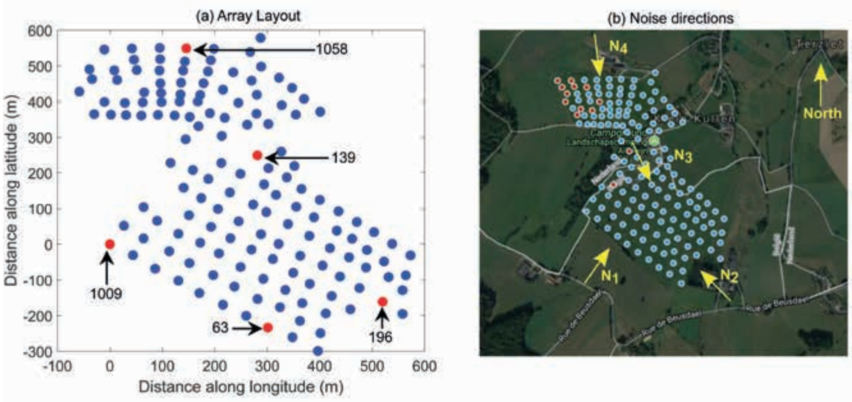

Figure 3 (a) Array layout showing location of sensor number 1009, 63, 139, 196 and 1058. (b) Map of the region showing the expected seismic noise sources.

configuration consisting of a low-power cryogenic interferometer optimized for low frequency band (ET-LF) and a higher power, room-temperature interferometer covering the high frequency band (ET-HF), which is an upscaled version of a second generation detector with the only differences being a length of 10 km and a circulating laser power of 3 MW. Unlike ET-HF, the low frequency xylophone interferometer ET-LF requires several innovations in technology. The main feature of ET-LF would be a reduction in the thermal noise by using cryogenic test masses, which is made possible by reducing the optical power to 18 kW. The other two sources of noise that limit the detector sensitivity are seismic and Newtonian noise. Apart from directly shaking the test masses via the suspension (seismic noise), the seismic displacement and density fluctuations of the subsurface due to seismic wave propagation couples to the suspended elements of the detector through gravitational forces of attraction and is referred to as the Newtonian noise. The resulting noise budget of ET-LF, limited by Newtonian noise at low frequencies and quantum noise at all other frequencies is shown in Figure 1(b). The contribution of seismic noise to ET noise budget can be reduced by several orders of magnitude by building the telescope in a region of low seismic activity and implementation of techniques in seismic isolation (Acernese et al., 2010). However, reducing the effect of Newtonian noise can be only accomplished by building the detector underground, where a significant reduction of seismic surface wave magnitudes can be accomplished. Limburg, a province in the south of The Netherlands is a candidate site for building the ET together with Belgium and Germany as the other two host nations. For recording the first underground seismic motion at the site, a 300 m-deep borehole is being drilled in the region alongside several other passive and active seismic campaigns that can help to characterize the shallow geology of the region up to depths of 300 m. In urban situations, using passive seismic tools is a suitable method for imaging the shallow subsurface. In this article we present the seismic interferometry results from a dense array deployed surrounding the borehole site.

Seismic noise interferometry

Seismic interferometry is a method to retrieve the seismic response of the medium between two receivers while treating one of them as a virtual source and the other as the receiver and vice-versa. It was first proposed by Claerbout in 1968 that auto-correlating the transmission response recorded at a receiver on the Earth's surface from noise sources in the subsurface, one would retrieve the reflection response at this receiver from a virtual source also at the same location. The method, however, gained much popularity in the exploration seismic community in the early 2000s due to works of Campillo and Paul (2003), who applied this method to earthquake coda-waves. Shapiro and Campillo (2004) demonstrated the use of this method for ambient seismic noise. Wapenaar (2004) formally proved the retrieval of elastodynamic Green's function of the medium using the method of cross-correlating seismic noise field at two receivers. Following Wapenaar and Fokkema (2006), given the measured velocity fields v_p, v_q at two receiver locations (x_A, x_B) respectively, the Green's function response of the medium can be approximated as

$$2R\left\{G^{v,f}_{p,q}\left(x_A,x_B,\omega\right)\right\}S\left(\omega\right)=\frac{2}{\rho c_p}\langle v_p^{*}\left(x_A,\omega\right)v_q\left(x_B,\omega\right)\rangle \qquad (1)$$

where $G^{f,v}_{p,q}\left(x_A,x_B,\omega\right)$ is the Fourier transform of the causal time domain Green's function due to source at x_B and receiver at x_A. The superscripts (v, f) represent the observed quantities like the particle velocity and the body force in this case and the subscripts (p, q) represent the components of each of these quantities. The density and P-wave velocity are represented as p and c_p respectively, $S(w)$ is the Fourier amplitude of the source function, $\langle\rangle$ denotes the ensemble average, and " * " denotes the complex conjugate.

Equation 1 is very suitable for practical implementation. It involves cross-correlating the velocity fields observed at two receivers and then performing an ensemble average, which yields the Green's function response of the medium. However, there are a few caveats to the implementation. The noise sources in reality are never distributed isotropically and constructing a closed surface that encloses the receiver pair might not be possible. Secondly, we assume that source strength from all sources is equal for all frequencies which might not be the case. Methods such as spectral whitening are useful in mitigating broad imbalances in the source spectra between noise sources. However, a persistent noise source originating at a certain azimuth might be existent in the region. In such a case the process of averaging would make one source dominant over the others even if spectral whitening of the observed velocity fields is performed prior to cross-correlation.

For our field studies, a reconnaissance passive seismic survey was conducted which revealed dominant noise propagating along the north-south direction (Koley et al., 2018). Apart from deciphering the noise propagation direction at the site, this study also gave us an estimate of the Rayleigh wave phase and group velocities in the region for the frequency band 2.6-8.0 Hz. We later make use of these results to verify the accuracy of the group velocity curves estimated using the surface wave Green's functions between receiver pairs.

Seismic noise characteristics

An array of 160 wireless 5 Hz vertical component geophones developed by Innoseis BV was deployed at Terziet, Limburg following the layout shown in Figure 2(a). Seismic noise was measured continuously from 19 December, 2017 to 10 January, 2018. Sensors were deployed approximately on a regular grid with an approximate grid size of 45-50 m. The sensor separation was decided based on the total number of sensors available and also the area of the survey region. While at high frequencies the phase velocity estimate from the empirical Green's function can suffer from cycle skipping due to too high receiver spacing of 50 m, the group velocity estimate between station pairs would be accurate. At low frequencies between 2.5-3.5 Hz, the maximum sensor separation of 900 m is sufficient for well-resolved group velocity extraction. Figure 2(b) shows the PSD averaged over 10-minute windows for the entire day of measurement on 20 December, 2017. For clarity we plot the PSD of only three of the nodes, and they are marked in Figure 2(a). Alongside, the power spectral density (PSD) of the seismic ground velocity measured at the nearby KNMI seismological observatory in Heijmansgroeve (HGN), Limburg (positioned at a depth of 10 m below the earth's surface) is also plotted. The wireless geophones are sensitive to frequencies > 0.2 Hz. Hence the primary microseismic peak recorded by our sensors below 0.1 Hz does not match with that measured at a HGN station. A perfect match is observed between the measured PSD at the HGN station and that of the Innoseis sensors in the secondary microseismic frequency band (0.2-1.0 Hz). However, the PSDs measured at frequencies >1 Hz do not match. We see a significant reduction in seismic noise measured at the KNMI station in comparison to our seismic measurements. The reduced magnitude of high frequency noise at KNMI station is due to its measurement at the

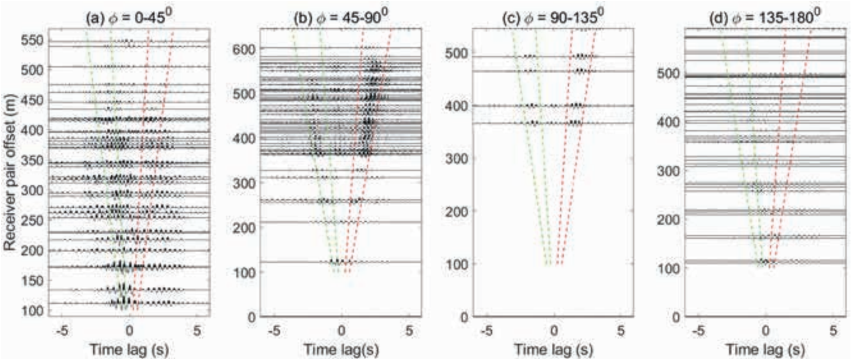

Figure 4 2.0-5.0 Hz bandpassed CCFs with sensor id 1009 as the reference station and one-way station pair azimuth in bins of 45°.

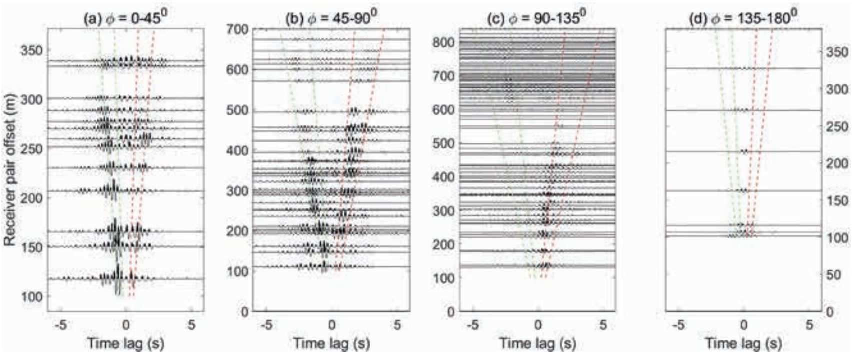

Figure 5 (a) 2.0-5.0 Hz bandpassed CCFs with sensor id 63 as the reference station and one-way station pair azimuth in bins of 45°.

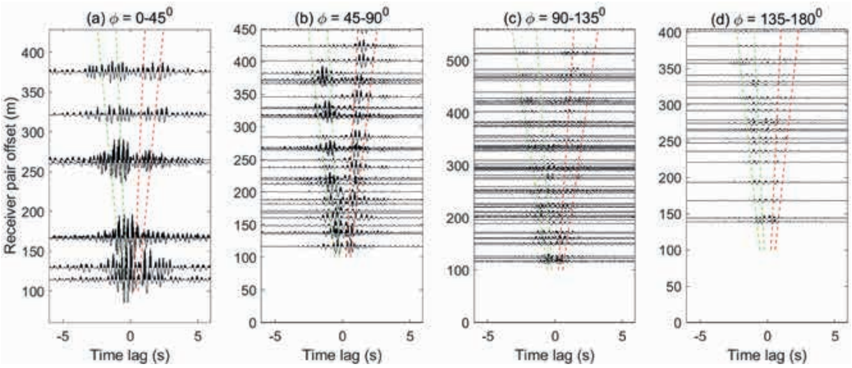

Figure 6 (a) 2.0-5.0 Hz bandpassed CCFs with sensor id 139 as the reference station and one-way station pair azimuth in bins of 45°.

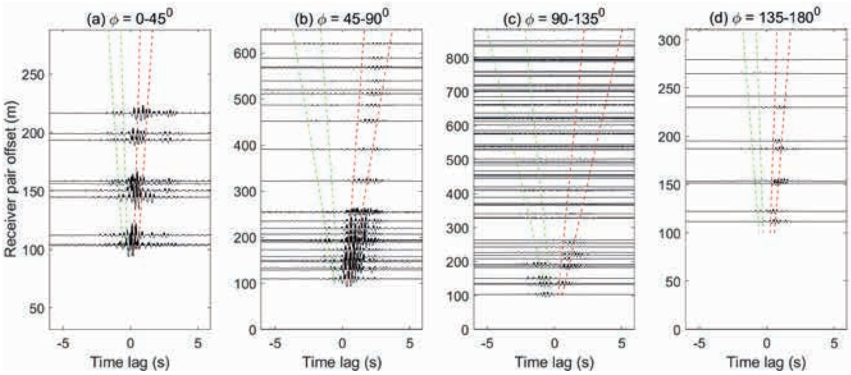

Figure 7 2.0-5.0 Hz bandpassed CCFs with sensor id 1058 as the reference station and one-way station pair azimuth in bins of 45°.

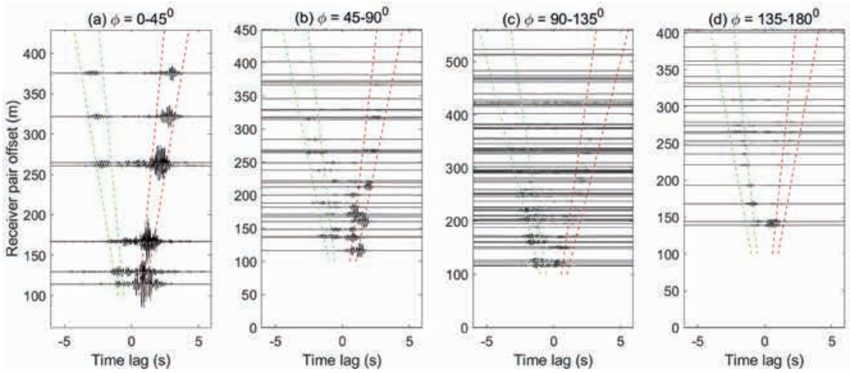

Figure 8 5.0-8.0 Hz bandpassed CCFs with sensor id 139 as the reference station and one-way station pair azimuth in bins of 45°.

bedrock. High frequency surface waves are sensitive to shallow structures, and attenuate exponentially as a function of the depth of propagation.

Green's function extraction

Continuous seismic noise records need to be preprocessed before the data can be used for computing the Green's function response between receiver pairs. Data from all the sensors are first extracted in one-hour segments and the methodology described below is implemented on one-hour data segments for all the sensors. Data is first de-trended followed by instrument response deconvolution. The field data is acquired at a high sampling rate of 250 Hz, and are downsampled to 25 Hz before we proceed any further. Subsequently, we also apply a low-cut filter with a cut-off frequency of 1 Hz. This is done to remove the effect of microseismic noise from the time-domain cross-correlations. This step is succeeded by temporal normalization and spectral whitening. Since the last two steps manipulate the amplitude of the signal, their order of execution must be respected (Bensen et al., 2007).

We then compute the time domain cross-correlation function (CCF) for all receiver pairs in order to extract the Green's function response of the medium. CCFs are evaluated for both positive and negative time lags up to a maximum of 40 seconds. The one-hour CCFs per receiver pair are then stacked for all hours of a day and subsequently for all 21 days of measurement. A total of 146 sensors recorded good quality data, hence we have a total of 10,585 stacked CCFs. From the reconnaissance survey we are already aware of the presence of strongly directional persistent noise sources at the site. Consequently, this phenomenon should also be strongly visible in the time domain CCFs. We devise a strategy to visualize the impact of directive noise in the CCFs. We select five stations in the entire field as reference stations with the sensor ids 1009, 63, 139, 196 and 1058 as marked in Figure 3a. The selection of these particular sensors is arbitrary with the only attribute that they span the entire field. Hence, visualizing the

CCFs corresponding to these sensors as the reference station will help us to understand the noise illumination pattern of the entire field. CCFs corresponding to each of these sensors are extracted from among all the CCFs and then binned using the inter-station azimuth. This implies that the CCFs are plotted as a function of receiver pair offset after segregating it into four one-way azimuthal bins. The bins run from 0°-180° at an interval of 45°. The azimuth is measured anticlockwise with respect to the east. Since the noise directions are also functions of the frequency of the propagating wavefield, we divide our analysis into two frequency bins. The CCFs are bandpass filtered in two frequency bands: A low frequency band between 2.0-5.0 Hz and a high frequency band between 5.0 and 8.0 Hz.

- Low frequency (2.0-5.0 Hz):

  Figure 4(a)-(d) shows the CCFs corresponding to sensor 1009 segregated into four azimuthal bins as mentioned earlier. The red and the green dotted lines have constant velocity slopes corresponding to 400 m/s and 175 m/s. These velocity limits serve as markers corresponding to the highest and lowest group velocities in the frequency band 2.0-5.0 Hz. CCFs in the azimuth range 45°-135° lie within the desired velocity ranges marked by the green and red lines corresponding to causal and acausal times and can be attributed to noise source N_1 (Figure 3b). CCFs in the azimuth range 0°-45° show spurious events that do not line up along the expected arrival times. A low signal to SNR is observed for station pairs in the azimuth bin 135°-185°. Figure 5 shows the extracted CCF with respect to sensor 63. This also shows a similar pattern as observed for sensor 1009 with an extra addition is the presence of well aligned events in the azimuth bin 0°-45° due to the noise source N_2 originating from the castle in the vicinity of sensor 63. However, the impact of the noise source N2 is not observed at higher offsets. Figure 6 shows the CCFs with reference sensor 139 shows the impact of noise source N_1 and N_3 simultaneously impinging the receiver pairs and is visible in the symmetric CCFs in the azimuth bin 45° - 90°. CCFs in the azimuth range 90° - 180°are a result of imperfect cancellation of the impinging noise wavefield. The CCFs with sensor 1058 (Figure 7) as the reference station is a typical case of asymmetric Green's function. Noise source N_4 originating north of the array dominate the noise field and result in one-sided CCFs. Well aligned events are observed for all azimuth bins. It implies that the noise source has a semi-circular azimuthal distribution running anticlockwise from east to west. Although the SNR of the CCFs fall as the receiver pair offset increases especially in the azimuth bin 90°-135°, but a closer examination shows a consistent arrival time of the surface waves.

  Studying the low frequency behaviour of the CCFs using the four reference stations, we conclude that low frequency noise propagation is dominantly along a north-south direction due to sources N_1 and N_4. Noise source N_2 and N_3 contribute mostly to small receiver pair offsets.

- High frequency (5.0-8.0 Hz):

  For analysing high-frequency surface wave Green's function we apply a 5.0-8.0 Hz bandpass filter to the CCFs. The effect of noise source N_1 and N_4 on the extracted CCFs is similar to what was observed in the low-frequency analysis. However, the impact of noise source N_2 and N_3 is more pronounced in the high-frequency regime and hence we present the resulting CCFs with respect to stations 139 and 196. CCFs for station 139, which is located close to the camping Allelijn, is shown in Figure 8. Azimuth bin 0°-45° show well aligned events with a high SNR due to close proximity to the source N_3. In

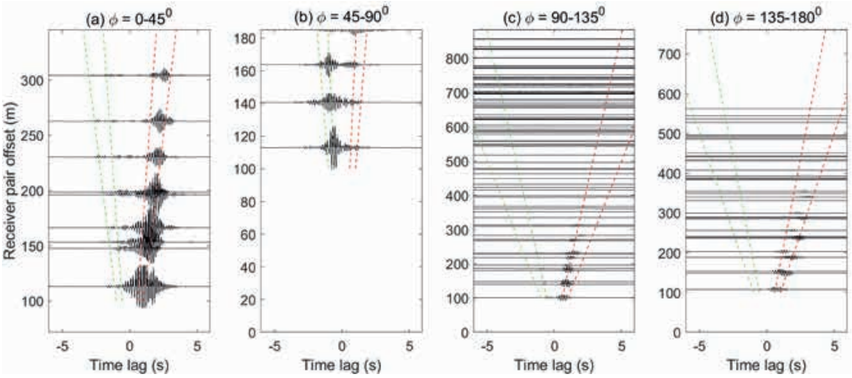

Figure 9 5.0-8.0 Hz bandpassed CCFs with sensor id 196 as the reference station and one-way station pair azimuth in bins of 45°.

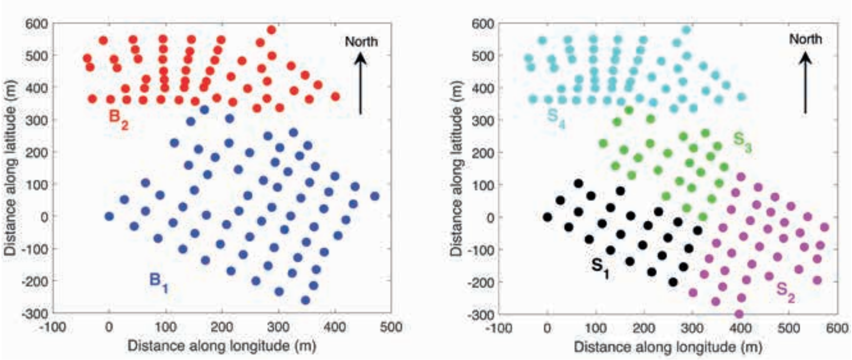

Figure 10 Array layout showing subarray B_1 and B_2 used for CCBF of low frequencies 2.5-5.0 Hz. (b) Subarray S_1, S_2, S_3 and S_4 used for CCBF of high frequencies 5.0-9.0 Hz.

the 45°-90° band, some events are well aligned and some are not. This is due to the way in which we bin the CCFs. A closer examination shows that events in the azimuth band 45°-60° are well aligned, and it is only in the range 65°-90° that show incorrect group travel times. A drop in the SNR of the CCFs is observed for receiver pair offsets >300 m (Figures 8c and 8d). Figure 9 shows the CCFs with sensor 196 as the reference station. This part of the field is illuminated strongly due to noise source N_2. Owing to dominant contribution from noise source $N_{2,}$ CCFs are one-sided and show high SNR up to offsets of 300 m. CCFs also show consistent travel times for all receiver pair azimuth.

Cross-correlation beamforming

Cross-correlation beamforming (CCBF) is a method of estimating the local direction and slowness of an incident plane wave on an array of sensors using the CCFs extracted from the receiver pairs.

If $CC_n(w_j)$ is the frequency domain CCF between i^{th} receiver pair in the n^{th} frequency bin, then the beampower BP for N such pairs is expressed as

$$BP\left(p_k, \theta_k, \omega_j\right) = \left|\sum_{n=1}^{N} CC_n\left(\omega_j\right) e^{i\omega_j d_n p_k coscos\left(\theta_n - \theta\right)}\right| \quad (2)$$

where d_n is the offset and θ_n the azimuth for the n^{th} receiver pair. Equation 2 is evaluated for all possible values of (p, θ) and the (p, θ) couple that maximizes the beampower BP gives an estimate of the dominant noise direction and slowness. In our analysis, we are interested in finding the local noise direction and hence we divide the seismic array into subarrays. Larger subarrays are preferred for low frequencies and smaller for high frequencies. Figure 10a shows the two subarrays labelled B_1 and B_2 used for analysing frequencies in the range 2.5-4.5 Hz. The frequency range 4.5-8.0 Hz is analysed using subarrays S_1, S_2, S_3 and S_4 as

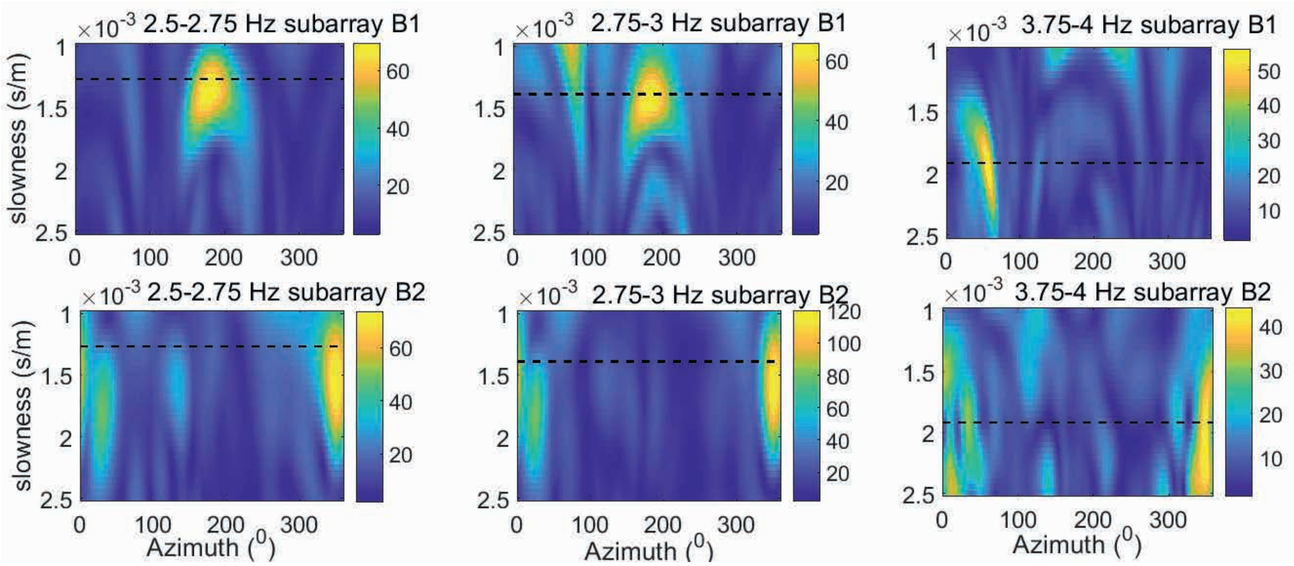

Figure 11 CCBF beampower plotted as a function of slowness and azimuth corresponding to subarray B_1 and B_2 in specified frequency bands. The dotted line shows the expected phase slowness as observed from the reconnaissance survey.

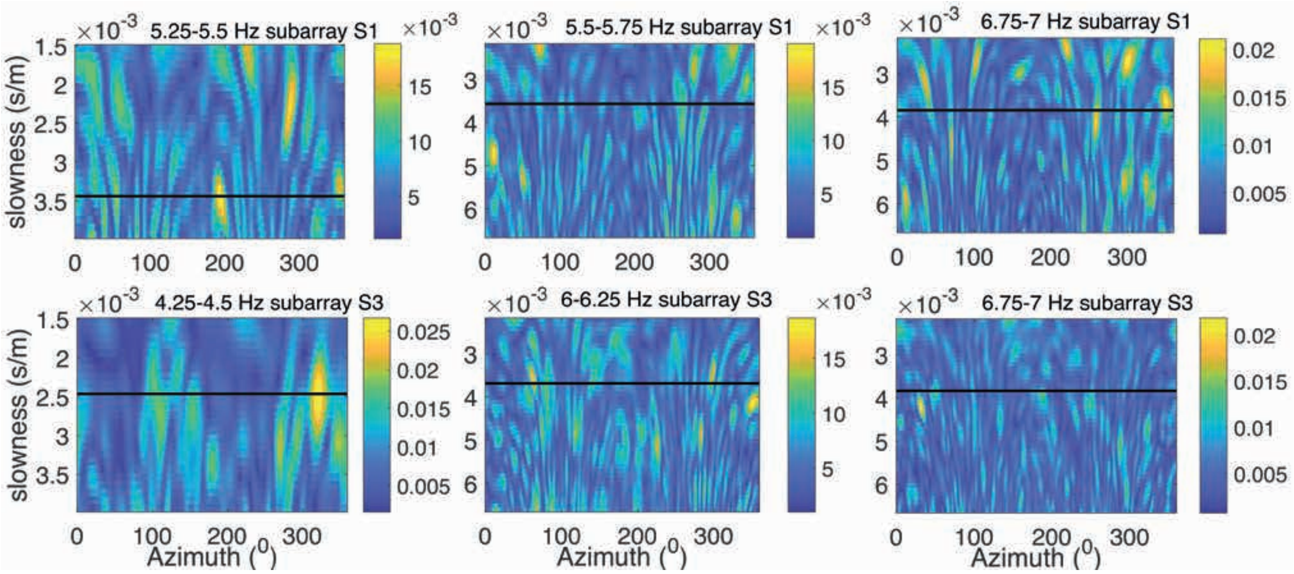

Figure 12 CCBF beampower plotted as a function of slowness and azimuth corresponding to subarray S_1 and S_2 for the high-frequency bands. The dotted line shows the expected phase slowness as observed from the reconnaissance survey.

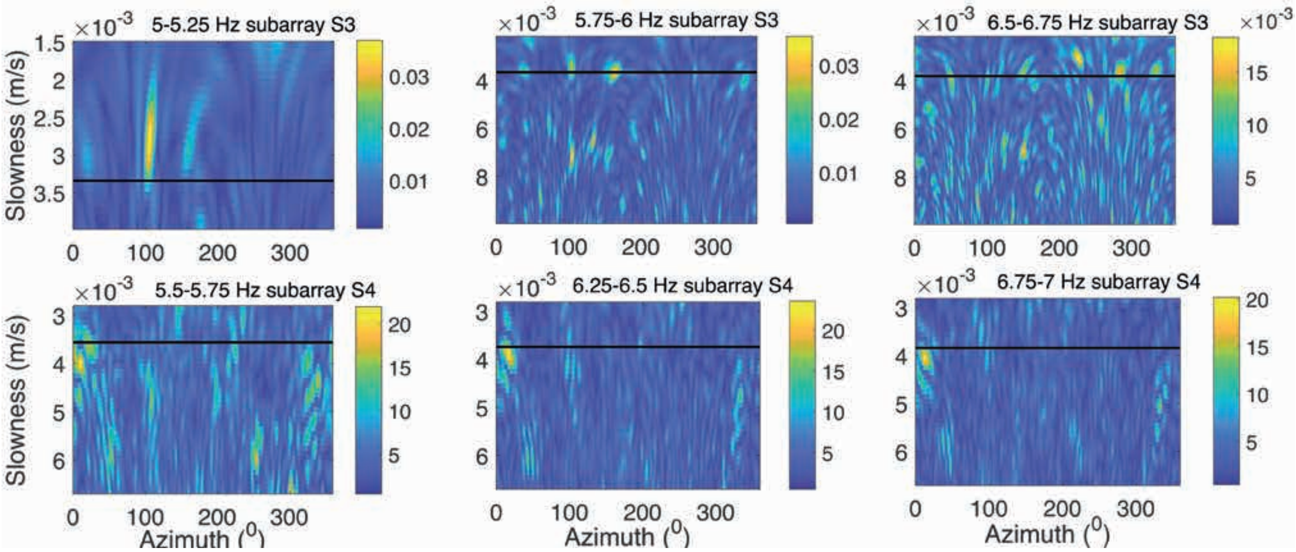

Figure 13 CCBF beampower plotted as a function of slowness and azimuth corresponding to subarray S_2 and S_4 for the high frequency bands. The dotted line shows the expected phase slowness as observed from the reconnaissance survey.

shown in Figure 10b. Figure 11a shows the beamforming results for subarray B_1 in the frequency band 2.5-4.5 Hz. A noise source originating from an azimuth of 180°-200° (same as in N_1 in Figure 3b) is observed. While subarray B_2 shows a noise source originating north at azimuths between 340°-360°, which is due to noise source N_4.

At high frequencies between 4.5-8 Hz, we subdivide our array into four subarrays. Figure 12 shows the CCBF results for array S_1 and S_3. In the frequency band 4.5-55 Hz, the noise impinging subarray S_1 is mainly from the south, whereas at frequencies >5.5 Hz, noise originate from the north, which is the same as N_3 shown in Figure 3b. For subarray S_3 the dominant source of noise is N_3 and some noise originating between azimuths 70° and 90° This contribution of the later source becomes more prominent at high frequencies. For subarray S_2 at high frequencies, we already established that a noise source originating from the castle at azimuths between 90° and 160° (N_2 in Figure 3b) dominates the extracted CCFs. This is also observed in the CCBF results in Figure 13. For subarray $S_{2,}$ noise N_4 dominates the high frequency band of the CCFs similar to what was observed for low frequencies. The high-frequency noise direction shifts slightly to north-north-east with increasing frequency unlike the low frequencies.

We have now quantitatively interpreted the dominant noise propagation direction as a function of the source-receiver location and frequency. Hence, selection of station pairs that are aligned along the local noise propagation direction is possible and we can estimate the group velocity for these station pairs.

Group velocity extraction

The group velocities as a function of frequency are extracted using the frequency-time analysis (FTAN) method (Levshin, 1972). However, not all station pairs yield the correct group velocity estimates. We impose three restrictions on the station pair selection for which the group velocities are extracted. First, a threshold of 15 is set on spectral SNR following Bensen et al. (2007). The spectral SNR is computed for every 0.1 Hz frequency band in the interval 2.5-8.0 Hz. Secondly, we set a limit on the ratio of the station separation and the wavelength corresponding to the extracted group velocity. Frequencies with wavelengths greater than three times the station separation are discarded from the analysis. Hence for low frequencies, station pairs that yield a reliable estimate of the group estimate are relatively less as compared to high frequencies. The third criterion is based on the inter-station azimuth. We have already proved that the sources of noise are strongly directional and persistent only along certain azimuths. Using the observed direction of noise propagation from the CCBF method of the last section, station pairs aligned along these azimuths are accepted in the analysis. Figure 14 shows the picked group velocity histogram for station pairs satisfying the above three conditions.

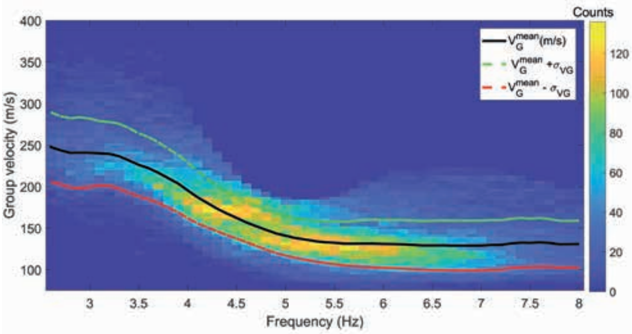

Figure 14 Estimated group velocity histogram with a bin width of 10 m/s with the mean (black solid curve) and one standard deviation limits shown using the green and red dashed curve.

Conclusion

Extracting the empirical Green's function of the medium by cross-correlating ambient noise recorded simultaneously by a receiver pair has been a well-known method since the early 2000s. This method works best for an isotropic distribution of the noise field and generally needs seismic noise recorded over several months to a year. Moreover, such studies mostly use the primary and the secondary microseismic energy as the source of noise. In this article we explored the use of seismic noise for extracting cross-correlations in the high-frequency regime. The main challenges in extracting reliable cross-correlation functions is the anisotropic distribution of the noise field and a degraded coherence at high frequencies for higher station pair separation. Cross-correlation beamforming was studied and implemented to understand the dominant noise propagation direction and facilitate accurate group velocity extraction between receiver pairs. Group velocities extracted using the group arrival times between receiver pairs give us insight into the geology of the region up to a maximum depth of 80 m.

References

Acernese, F., Amico, P., Arnaud, N., Babusci, D., Barillé, R., Barone, F., Barsotti, L., Barsuglia, M., Beauville, F. and Bizouard, M. [2004]. Properties of seismic noise at the Virgo site. *Classical and Quantum Gravity*, **21**, S433.

Acernese, F., Antonucci, F., Aoudia, S., Arun, K., Astone, P., Ballardin, G., Barone, F., Barsuglia, M., Bauer, T.S. and Beker, M. [2010]. Measurements of superattenuator seismic isolation by Virgo interferometer. *Astroparticle Physics*, **33**, 182–189.

Bensen, G., Ritzwoller, M., Barmin, M., Levshin, A, Lin, F., Moschetti, M., Shapiro, N. and Yang, Y. [2007]. Processing seismic ambient noise data to obtain reliable broad-band surface wave dispersion measurements. *Geophysical Journal International*, **169**, 3, 1239–1260.

Campillo, M. and Paul, A. [2003]. Long-range correlations in the diffuse seismic coda. *Science*, **299**, 5606, 547–549.

Claerbout, J.F. [1968]. Synthesis of a layered medium from its acoustic transmission response. *Geophysics*, **33**, 2, pp. 264–269.

Freise, A., Chelkowski, S., Hild, S., Del Pozzo, W., Perreca, A. and Vecchio, A. [2009]. Triple Michelson interferometer for a third-generation gravitational wave detector. *Classical and Quantum Gravity*, **26**, 8, 085012.

Freise, A., Hild, S., Somiya, K., Strain, K.A., Vicere, A., Barsuglia, M. and Chelkowski, S. [2011]. Optical detector topology for third-generation gravitational wave observatories. *General Relativity and Gravitation*, **43**, 2, 537–567.

Hild, S., Abernathy, M., Acernese, F., Amaro-Seoane, P., Andersson, N., Arun, K., Barone, F., Barr, B., Barsuglia, M. and Beker, M. [2011]. Sensitivity studies for third-generation gravitational wave observatories. *Classical and Quantum Gravity*, **28**, 9, 094013.

Koley, S., Campman, X., Bader, M., Bulten, H., Brand, J., Linde, F. and Beker, M. [2018]. Seismic noise characterization at a potential site for the Einstein telescope underground gravitational wave detector. 80th EAGE Conference and Exhibition.

L.S. Collaboration and V. Collaboration [2018]. Gwtc-1: A gravitational-wave transient catalog of compact binary mergers observed by LIGO and VIRGO during the first and second observing runs. arXiv preprint arXiv:1811.12907.

Levshin, A., Pisarenko, V. and Pogrebinsky, G. [1972]. Frequency-time analysis of oscillations. *Annales de Geophysique*, **28**, 211.

Puntoro, M., Abernathy, M., Acernese, F., Allen, B., Andersson, N., Arun, K., Barone, F., Barr, B., Barsuglia, M. and Beker, M. [2010]. The Einstein telescope: a third-generation gravitational wave observatory. *Classical and Quantum Gravity*, **27**, 19, p. 194002.

Shapiro, N.M. and Campillo, M. [2004]. Emergence of broadband Rayleigh waves from correlations of the ambient seismic noise. *Geophysical Research Letters*, **31**, 7.

Wapenaar, K. [2004]. Retrieving the elastodynamic Green's function of an arbitrary inhomogeneous medium by cross correlation. *Physical review letters*, **93**, 25, 254301.

Wapenaar, K. and Fokkema, J. [2006]. Green's function representations for seismic interferometry. Geophysics, **71**, 4, SI33–SI46.